A Letters Journal Exploring the Frontiers of Physics

July 2020

EPL, **131** (2020) 24002
doi: 10.1209/0295-5075/131/24002

www.epljournal.org

Effectively infinite thermal conductivity and zero-index thermal cloak

L. J. Xu[a], S. Yang and J. P. Huang[b]

Department of Physics, State Key Laboratory of Surface Physics, and Key Laboratory of Micro and Nano Photonic Structures (MOE), Fudan University - Shanghai 200438, China

received 8 May 2020; accepted in final form 6 July 2020
published online 20 August 2020

PACS 44.10.+i – Heat conduction
PACS 05.70.-a – Thermodynamics
PACS 81.05.Zx – New materials: theory, design, and fabrication

Abstract – Thermal conductivities are the key to heat transfer, and high thermal conductivities are generally beneficial and sometimes indispensable to design thermal metadevices. Therefore, the exploration of high thermal conductivities never stops. However, infinite thermal conductivities have not yet been discovered. To solve the problem, we propose an exact approach to effectively infinite thermal conductivities with a constant-temperature boundary condition, which can be easily realized by an external thermostatic sink. Since (effectively) infinite thermal conductivities just correspond to zero refractive indexes in photonics, they have direct applications in designing zero-index thermal metadevices. For example, we experimentally demonstrate zero-index thermal cloaks which can work in highly conductive backgrounds with simple structures. These results provide insights into thermal metadevices and thermal management with effectively infinite thermal conductivities.

Introduction. – Thermal conductivities play a crucial role in heat transfer, and extreme (zero and infinite) thermal conductivities are always a research focus due to their excellent properties. For low thermal conductivities, a recent study reported that the thermal conductivity of ceramic aerogel can be as low as $0.0024\,\mathrm{W\ m^{-1}\ K^{-1}}$ [1]. For high thermal conductivities, there is still a long way ahead. Although many materials have high thermal conductivities, such as boron nitride with $600\,\mathrm{W\ m^{-1}\ K^{-1}}$ [2], carbon nanotube with $2300\,\mathrm{W\ m^{-1}\ K^{-1}}$ [3], and graphene with $5300\,\mathrm{W\ m^{-1}\ K^{-1}}$ [4], they are still far from infinite thermal conductivities.

To overcome the difficulty, a recent study reported that the effective thermal conductivity of a moving fluid can approximately tend to infinity [5]. Such an effectively infinite thermal conductivity requires the velocity of the moving fluid to be also infinite, which cannot be exactly realized. To go further, here we propose an exact approach to effectively infinite thermal conductivities with even simpler structures. That is, by applying a constant-temperature boundary condition on an object with a finite thermal conductivity, the object can have an effectively infinite thermal conductivity. Meanwhile, the constant-temperature boundary condition can be easily realized by an external thermostatic sink, which is beneficial for practical applications.

Since (effectively) infinite thermal conductivities are in analogy of zero refractive indexes in photonics [6–12], they can be used to design zero-index thermal metadevices. We take thermal cloaking [13–26] as an example which can be realized by transformation thermotics [13–16], bilayer scheme [17–22], or scattering cancellation [23,24]. Here we use effectively infinite thermal conductivities to realize zero-index thermal cloaks, which can work in highly conductive backgrounds with simple structures. Concretely speaking, if the previous bilayer scheme [17–22] is applied to a highly conductive background (such as copper, $400\,\mathrm{W\ m^{-1}\ K^{-1}}$), the thermal conductivity of the inner shell is zero, and that of the outer shell should be larger than $400\,\mathrm{W\ m^{-1}\ K^{-1}}$. However, few common materials have thermal conductivities higher than $400\,\mathrm{W\ m^{-1}\ K^{-1}}$ [5]. Although some rare materials like diamond have high thermal conductivities, the cost and difficulty of practical applications also increase. By contrast, if the zero-index scheme is applied, the core with

[a] E-mail: 13307110076@fudan.edu.cn
[b] E-mail: jphuang@fudan.edu.cn

a constant-temperature boundary condition can have an effectively infinite thermal conductivity. Therefore, the thermal conductivity of the outer shell can be smaller than $400\,\mathrm{W\ m^{-1}\ K^{-1}}$, and many common materials like aluminum can be applied. Therefore, the zero-index scheme is free from the thermal conductivities of backgrounds.

Theory of effectively infinite thermal conductivity. – Thermal conduction is dominated by the Fourier law, namely $\boldsymbol{J} = -\kappa\boldsymbol{\nabla}T$, where $\boldsymbol{J}$ is heat flux, κ is thermal conductivity, and T denotes temperature. To understand the temperature effect of an infinite thermal conductivity, we put a two-dimensional elliptical particle (with thermal conductivity $\kappa_p = \infty$, actually set as $10^{10}\,\mathrm{W\ m^{-1}\ K^{-1}}$) in the background (with thermal conductivity κ_b) and apply a horizontal thermal field $\boldsymbol{K}_0$. As a result, the isotherms are all repelled, and the black arrows (denoting the directions of heat fluxes) are always perpendicular to the exterior boundary of the particle (see fig. 1(a)). Clearly, the particle is isothermal, and a brief proof is as follows. We denote the temperature distribution of the particle as T_p. By solving the Laplace equation $\boldsymbol{\nabla}\cdot(-\kappa\boldsymbol{\nabla}T) = 0$, we can derive T_p as

$$T_p = \frac{-\kappa_b}{L_{p1}\kappa_p + (1-L_{p1})\kappa_b}K_0 x_1 + T_0, \qquad (1)$$

where $K_0 = |\boldsymbol{K}_0|$, T_0 is reference temperature, and (x_1, x_2, x_3) denote the Cartesian coordinates. L_{p1} is the shape factor of the particle along the x_1-axis, which will be discussed later. Equation (1) indicates that whatever value L_{p1} takes on, if $\kappa_p = \infty$, T_p is always a constant T_0. Physically speaking, since heat fluxes ($\boldsymbol{J} = -\kappa\boldsymbol{\nabla}T$) do not diverge, a direct conclusion from $\kappa = \infty$ is $\boldsymbol{\nabla}T = 0$. In other words, a finite thermal conductivity with a constant-temperature boundary condition is equivalent to an infinite thermal conductivity. For comparison, we reset κ_p to a finite value ($\kappa_p < \infty$, actually set as $0.026\,\mathrm{W\ m^{-1}\ K^{-1}}$) and apply a constant-temperature boundary condition on the boundary of the particle (see fig. 1(b)). As a result, the temperature profile and directions of heat fluxes are the same as those in fig. 1(a), thus achieving an effectively infinite thermal conductivity with a constant-temperature boundary condition. Note that such an equivalence is only exact for temperature distributions.

Theory of zero-index thermal cloak. – Zero-index metadevices have been widely studied to manipulate electromagnetic waves [6–12] and acoustic waves [27–30] due to their excellent properties. We know that the directions of heat fluxes are always perpendicular to the exterior boundary of the particle with an (effectively) infinite thermal conductivity (see figs. 1(a) and (b)). This phenomenon is in accordance with that of zero refractive indexes in photonics where electromagnetic waves travel outward vertically from materials with zero refractive indexes. Therefore, (effectively) infinite thermal conductivities can be directly used to design zero-index thermal metadevices.

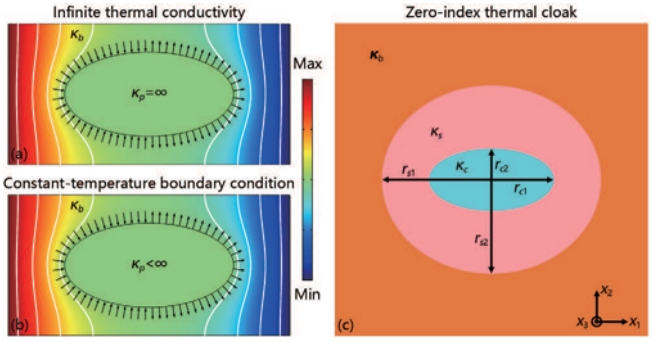

Fig. 1: (a) Temperature profile with an elliptical particle ($\kappa_p = \infty$, actually set as $10^{10}\,\mathrm{W\ m^{-1}\ K^{-1}}$) embedded in the background ($\kappa_b = 400\,\mathrm{W\ m^{-1}\ K^{-1}}$). (b) Temperature profile with a common particle ($\kappa_p < \infty$, actually set as $0.026\,\mathrm{W\ m^{-1}\ K^{-1}}$) and a constant-temperature boundary condition (with temperature (Max+Min)/2) embedded in the same background. Here Max and Min denote the temperatures of the left and right boundaries, respectively. Rainbow surfaces denote temperature distributions, and white lines represent isotherms. (c) Schematic diagram of zero-index thermal cloak. A constant-temperature boundary condition is applied on the boundary of the core, so the core has an effectively infinite thermal conductivity.

Zero-index thermal cloaks are a typical example of zero-index thermal metadevices, which can be realized by introducing thermal convection [5]. Such a scheme requires the velocity of moving fluid to be infinite which cannot be exactly realized, thus called near-zero-index thermal cloaks. In contrast, the present approach can realize exact-zero-index thermal cloaks with even simpler structures because only an external thermostatic sink is required to realize a constant-temperature boundary condition. In a word, thermal zero-index parameters indicate that thermal conductivities are (effectively) infinite. We apply a constant-temperature boundary condition on the core to realize an effectively infinite thermal conductivity, so the present thermal cloaks are also called zero-index thermal cloaks.

Zero-index thermal cloaks are essentially a core-shell structure (see fig. 1(c)). We denote the thermal conductivities of the core and shell as κ_c and κ_s, respectively. The subscript c (or s) represents the core (or shell) throughout this work. For generality, we consider an ellipsoidal case in three dimensions. The semiaxes of the core and shell along the x_i-axis ($i = 1, 2, 3$) are denoted as r_{ci} and r_{si}, respectively. The effective thermal conductivity of such a core-shell structure (denoted as $\boldsymbol{\kappa}_e$) is anisotropic, and the component along the x_i-axis (denoted as κ_{ei}) can be calculated by

$$\kappa_{ei} = \kappa_s\frac{L_{ci}\kappa_c + (1-L_{ci})\kappa_s + f(1-L_{si})(\kappa_c-\kappa_s)}{L_{ci}\kappa_c + (1-L_{ci})\kappa_s - fL_{si}(\kappa_c-\kappa_s)}, \qquad (2)$$

where $f = r_{c1}r_{c2}r_{c3}/(r_{s1}r_{s2}r_{s3})$ is core fraction. L_{ci} and L_{si} are, respectively, the shape factors of the core and shell

along the x_i-axis, which can be calculated by

$$L_{wi} = \frac{r_{w1}r_{w2}r_{w3}}{2} \times \int_0^\infty \frac{\mathrm{d}u}{(u+r_{wi}^2)\sqrt{(u+r_{w1}^2)(u+r_{w2}^2)(u+r_{w3}^2)}}. \quad (3)$$

Here the subscript w can take c or s, representing the shape factor of the core or shell. Note that only when the core-shell structure is concentric or confocal, can eq. (2) predict the effective thermal conductivities exactly.

When a constant-temperature boundary condition is applied, the thermal conductivity of the core turns to infinity, namely $\kappa_c = \infty$, as proved in figs. 1(a) and (b). Then, eq. (2) becomes

$$\kappa_{ei} = \kappa_s \frac{L_{ci} + f(1 - L_{si})}{L_{ci} - fL_{si}}. \quad (4)$$

Equation (4) can also be applied to two dimensions as long as we take $r_{w3} = \infty$ and $f = r_{c1}r_{c2}/(r_{s1}r_{s2})$. Then, eq. (3) can be reduced to $L_{w1} = r_{w2}/(r_{w1} + r_{w2})$, $L_{w2} = r_{w1}/(r_{w1} + r_{w2})$, and $L_{w3} = 0$. As an intrinsic property, $L_{w1} + L_{w2} + L_{w3} = 1$ is always valid no matter in two or three dimensions.

Simulations of zero-index thermal cloak. – We perform simulations with COMSOL Multiphysics (`http://www.comsol.com/`) to confirm these theoretical analyses. Without loss of generality, we discuss two two-dimensional cases including a circular one and an elliptical one. Figures 2(a) and (b) show the circular case where the thermal conductivities of the core and shell are $\kappa_c = 0.026$ and $\kappa_s = 203\,\mathrm{W\ m^{-1}\ K^{-1}}$, respectively. The thermal conductivity of the background is set as $\boldsymbol{\kappa}_b = \boldsymbol{\kappa}_e = 400\,\mathrm{W\ m^{-1}\ K^{-1}}$ which is derived from eq. (4). When a constant-temperature boundary condition is not applied, the isotherms are contracted due to the smaller effective thermal conductivity of the core-shell structure (see fig. 2(a)). However, if we apply a constant-temperature boundary condition on the boundary of the core, thermal cloaking can be achieved because the core has an effectively infinite thermal conductivity (see fig. 2(b)).

We further discuss the elliptical case with the same thermal conductivities of the core-shell structure, namely $\kappa_c = 0.026$ and $\kappa_s = 203\,\mathrm{W\ m^{-1}\ K^{-1}}$. Different from the circular case, the effective thermal conductivity of the elliptical core-shell structure is anisotropic. Therefore, we set the thermal conductivity of the background as $\boldsymbol{\kappa}_b = \boldsymbol{\kappa}_e = \mathrm{diag}(358, 270)\,\mathrm{W\ m^{-1}\ K^{-1}}$ (expressed in Cartesian coordinates) which is also derived from eq. (4). In the presence of a horizontal thermal field, the smaller effective thermal conductivity of the core-shell structure makes the isotherms contracted (see fig. 2(c)), whereas a constant-temperature boundary condition helps us achieve thermal cloaking (see fig. 2(d)). The results are similar if the system is in the presence of a vertical thermal field (see figs. 2(e) and (f)).

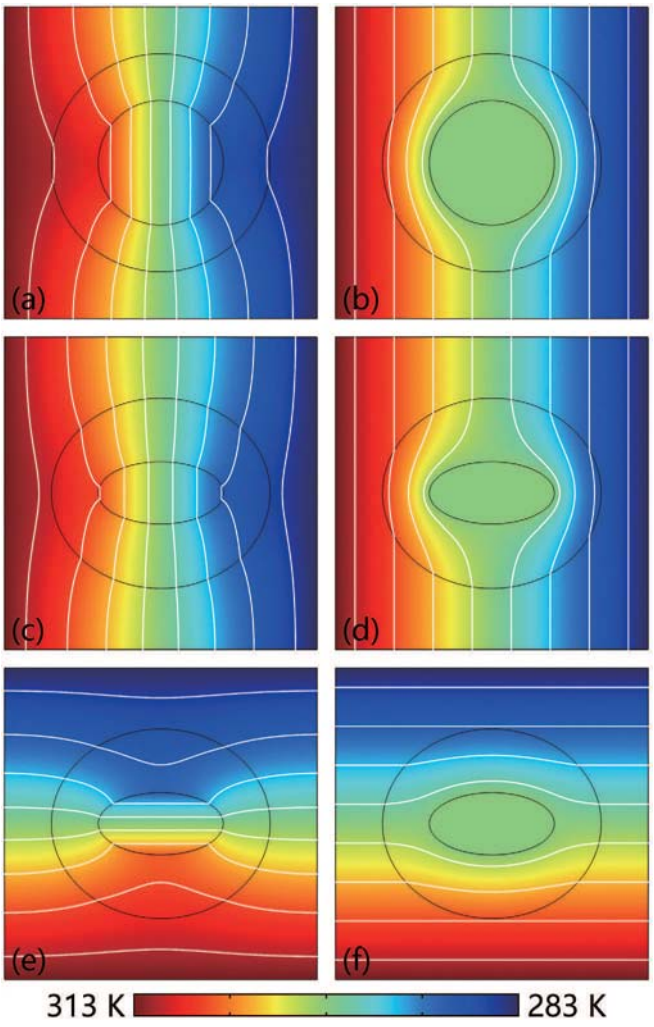

Fig. 2: Simulations of zero-index thermal cloak. The system size is $20 \times 20\,\mathrm{cm^2}$. The thermal conductivities of the core and shell are $\kappa_c = 0.026$ and $\kappa_s = 203\,\mathrm{W\ m^{-1}\ K^{-1}}$, respectively. The thermal conductivities of the background in (a)–(b) and (c)–(f) are $\boldsymbol{\kappa}_b = 400$ and $\boldsymbol{\kappa}_b = \mathrm{diag}(358, 270)\,\mathrm{W\ m^{-1}\ K^{-1}}$, respectively. The inner and outer radii of the shell in (a) and (b) are $r_{c1} = r_{c2} = 4$ and $r_{s1} = r_{s2} = 7\,\mathrm{cm}$, respectively. The inner and outer semiaxes of the elliptical shell in (c)–(f) are $r_{c1} = 4$, $r_{c2} = 2$, $r_{s1} = 7$, and $r_{s2} = 6\,\mathrm{cm}$, respectively. The left and right columns show the temperature profiles without and with a constant-temperature boundary condition, respectively. The constant-temperature boundary condition is set at 298 K. The high and low temperatures are set at 313 and 283 K, respectively. The other boundaries are insulated.

Experiments of zero-index thermal cloak. – For experimental demonstration, we fabricate six samples to confirm the six simulations in fig. 2. We use integrated fabrication technology, indicating that the samples have not weld joints. The three samples without a constant-temperature boundary condition are presented in figs. 3(a), (c), and (e). Air holes are drilled on the copper plate to realize the designed thermal conductivities of the shell and background. Another three samples

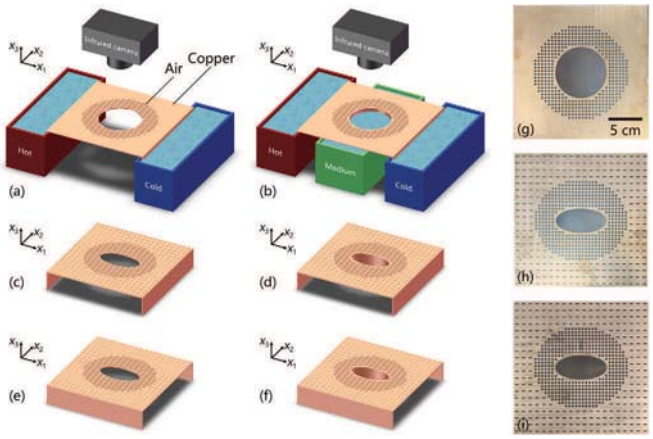

Fig. 3: Schematic diagrams of six samples and experimental setup. The thermal conductivities of air and copper are 0.026 and 400 W m^{-1} K^{-1}, respectively. The size of each sample is $20 \times 20 \times 4\,\mathrm{cm}^3$ with copper thickness of 2 mm. The central air hole in (a) and (b) has a radius of 4 cm, and that in (c)–(f) has semiaxes of $r_{c1} = 4$ and $r_{c2} = 2$ cm. The effective shell radius in (a) and (b) is 7 cm, and the effective shell semiaxes in (c)–(f) are $r_{s1} = 7$ and $r_{s2} = 6$ cm. The air holes in the shell regions in (a)–(f) have the same radius of 1.6 mm, thus making the effective thermal conductivity of the shells to be 203 W m^{-1} K^{-1}. The air holes in the background regions in (c)–(f) have a major semiaxis of 2.9 mm and a minor one of 0.8 mm, thus making the effective thermal conductivity of the backgrounds to be diag(358, 270) W m^{-1} K^{-1}. The distance between air holes in the shell region is 5 mm, and that in the background region is 10 mm. The temperatures of hot, medium, and cold sources are set at 313, 298, 283 K, respectively. (g)–(i) Real photos of (b), (d), and (f), respectively.

with a constant-temperature boundary condition are presented in figs. 3(b), (d), and (f). By immersing the central hollow cylinders in an external thermostatic sink with medium temperature, a constant-temperature boundary condition can be obtained and effectively infinite thermal conductivities are achieved. Compared with other active schemes [31–33], our scheme does not require complicated temperature settings. The upper and lower surfaces of these six samples are, respectively, covered with transparent plastic and foamed plastic to reduce environmental interferences. The real photos of figs. 3(b), (d), and (f) with top view are presented in figs. 3(g)–(i), respectively.

Then, we use the Flir E60 infrared camera to detect temperature distributions. The measured results corresponding to the six samples in fig. 3 are presented in the left two columns of fig. 4. We also perform finite-element simulations according to these six samples, and corresponding results are shown in the third and fourth columns of fig. 4. For quantitative analyses, we plot the temperature distributions at $x_1 = -8$ cm for the first two rows and $x_2 = -8$ cm for the last row (the origin is in the center of each simulation). The experiments and simulations agree well with each other (see figs. 4(m)–(o)), thus confirming the feasibility of realizing zero-index thermal cloaks with effectively infinite thermal conductivities.

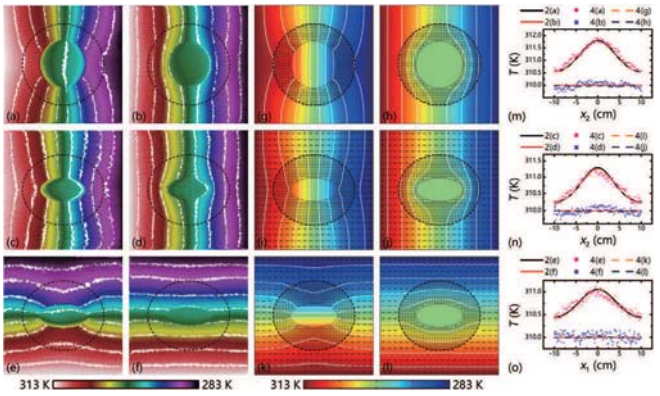

Fig. 4: Measured results (left two columns) and simulated results (the third and fourth columns) of the six samples in fig. 3. Dashed lines are plotted for the convenience of comparison. (m) and (n) show the temperature distributions at $x_1 = -8$ cm (the origin is in the center of each simulation), and (o) shows the temperature distributions at $x_2 = -8$ cm. Each line corresponds to a figure shown in the legend.

The cloaking effect is also robust under more complicated conditions such as different directions of external fields, point heat sources, and three dimensions. Furthermore, thermal cloaking can be extended to other functions such as thermal camouflaging [34–46]. Nevertheless, the scheme is applicable for only stable states because the temperature of a constant-temperature boundary condition is fixed.

Conclusion. – In summary, we have shown that by applying a constant-temperature boundary condition on a common material, an effectively infinite thermal conductivity can be exactly achieved. Meanwhile, the constant-temperature boundary condition can be easily realized by an external thermostatic sink. The present approach has direct applications in designing zero-index thermal cloaks which can work in highly conductive backgrounds with simple structures. These features such as accuracy and simplicity are beneficial to practical applications. This work applies a constant-temperature boundary condition to realize effectively infinite thermal conductivities, which is expected to design more zero-index thermal metadevices.

* * *

We acknowledge the financial support by the National Natural Science Foundation of China under Grant No. 11725521.

REFERENCES

[1] Xu X., Zhang Q. Q., Hao M. L., Hu Y., Lin Z. Y., Peng L. L., Wang T., Ren X. X., Wang C., Zhao Z. P., Wan C. Z., Fei H. L., Wang L., Zhu J., Sun H. T., Chen W. L., Du T., Deng B. W., Cheng G. J.,

Shakir I., Dames C., Fisher T. S., Zhang X., Li H., Huang Y. and Duan X. F., *Science*, **363** (2019) 723.
[2] Lindsay L. and Broido D. A., *Phys. Rev. B*, **84** (2011) 155421.
[3] Pop E., Mann D., Wang Q., Goodson K. and Dai H. J., *Nano Lett.*, **6** (2006) 96.
[4] Balandin A. A., Ghosh S., Bao W. Z., Calizo I., Teweldebrhan D., Miao F. and Lau C. N., *Nano Lett.*, **8** (2008) 902.
[5] Li Y., Zhu K. J., Peng Y. G., Li W., Yang T. Z., Xu H. X., Chen H., Zhu X. F., Fan S. H. and Qiu C. W., *Nat. Mater.*, **18** (2019) 48.
[6] Huang X. Q., Lai Y., Hang Z. H., Zheng H. H. and Chan C. T., *Nat. Mater.*, **10** (2011) 582.
[7] Maas R., Parsons J., Engheta N. and Polman A., *Nat. Photon.*, **7** (2013) 907.
[8] Wu Y. and Li J. C., *Appl. Phys. Lett.*, **102** (2013) 183105.
[9] Li Y., Kita S., Munoz P., Reshef O., Vulis D. I., Yin M., Loncar M. and Mazur E., *Nat. Photon.*, **9** (2015) 738.
[10] Alam M. Z., Leon I. D. and Boyd R. W., *Science*, **352** (2016) 795.
[11] Alam M. Z., Schulz S. A., Upham J., Leon I. D. and Boyd R. W., *Nat. Photon.*, **12** (2018) 79.
[12] Chu H. C., Li Q., Liu B. B., Luo J., Sun S. L., Hang Z. H., Zhou L. and Lai Y., *Light-Sci. Appl.*, **7** (2018) 50.
[13] Fan C. Z., Gao Y. and Huang J. P., *Appl. Phys. Lett.*, **92** (2008) 251907.
[14] Chen T. Y., Weng C. N. and Chen J. S., *Appl. Phys. Lett.*, **93** (2008) 114103.
[15] Xu L. J., Dai G. L. and Huang J. P., *Phys. Rev. Appl.*, **13** (2020) 024063.
[16] Xu L. J., Yang S., Dai G. L. and Huang J. P., *ES Energy Environ.*, **7** (2020) 65.
[17] Xu H. Y., Shi X. H., Gao F., Sun H. D. and Zhang B. L., *Phys. Rev. Lett.*, **112** (2014) 054301.
[18] Han T. C., Bai X., Gao D. L., Thong J. T. L., Li B. W. and Qiu C. W., *Phys. Rev. Lett.*, **112** (2014) 054302.
[19] Ma Y. G., Liu Y. C., Raza M., Wang Y. D. and He S. L., *Phys. Rev. Lett.*, **113** (2014) 205501.
[20] He X., Yang T. Z., Zhang X. W., Wu L. Z. and He X. Q., *Sci. Rep.*, **7** (2017) 16671.
[21] Han T. C., Yang P., Li Y., Lei D. Y., Li B. W., Hippalgaonkar K. and Qiu C. W., *Adv. Mater.*, **117** (2018) 1804019.
[22] Xu L. J. and Huang J. P., *Phys. Rev. Appl.*, **12** (2019) 044048.
[23] Farhat M., Chen P. Y., Bagci H., Amra C., Guenneau S. and Alù A., *Sci. Rep.*, **5** (2015) 9876.
[24] Farhat M., Guenneau S., Chen P. Y., Alù A. and Salama K. N., *Phys. Rev. Appl.*, **11** (2019) 044089.
[25] Hu R., Xie B., Hu J. Y., Chen Q. and Luo X. B., *EPL*, **111** (2015) 54003.
[26] Li J. X., Li Y., Li T. L., Wang W. Y., Li L. Q. and Qiu C. W., *Phys. Rev. Appl.*, **11** (2019) 044021.
[27] Zheng L. Y., Wu Y., Ni X., Chen Z. G., Lu M. H. and Chen Y. F., *Appl. Phys. Lett.*, **104** (2014) 161904.
[28] Liu F. M. and Liu Z. Y., *Phys. Rev. Lett.*, **115** (2015) 175502.
[29] Dubois M., Shi C. Z., Zhu X. F., Wang Y. and Zhang X., *Nat. Commun.*, **8** (2017) 14871.
[30] Xu C. Q., Ma G. C., Chen Z. G., Luo J., Shi J. J., Lai Y. and Wu Y., *Phys. Rev. Lett.*, **124** (2020) 074501.
[31] Nguyen D. M., Xu H. Y., Zhang Y. M. and Zhang B. L., *Appl. Phys. Lett.*, **107** (2015) 121901.
[32] Guo J. and Qu Z. G., *Int. J. Heat Mass Transfer*, **127** (2018) 1212.
[33] Xu L. J., Yang S. and Huang J. P., *Phys. Rev. E*, **100** (2019) 062108.
[34] Li Y., Bai X., Yang T. Z., Luo H. and Qiu C. W., *Nat. Commun.*, **9** (2018) 273.
[35] Hu R., Zhou S. L., Li Y., Lei D. Y., Luo X. B. and Qiu C. W., *Adv. Mater.*, **30** (2018) 1707237.
[36] Zhou S. L., Hu R. and Luo X. B., *Int. J. Heat Mass Transfer*, **127** (2018) 607.
[37] Hu R., Huang S. Y., Wang M., Zhou L. L., Peng X. Y. and Luo X. B., *Phys. Rev. Appl.*, **10** (2018) 054032.
[38] Yang S., Xu L. J. and Huang J. P., *EPL*, **126** (2019) 54001.
[39] Yang S., Xu L. J. and Huang J. P., *EPL*, **128** (2019) 34002.
[40] Hu R., Huang S. Y., Wang M., Luo X. L., Shiomi J. and Qiu C. W., *Adv. Mater.*, **31** (2019) 1807849.
[41] Xu L. J., Yang S. and Huang J. P., *Phys. Rev. Appl.*, **11** (2019) 054071.
[42] Peng X. Y. and Hu R., *ES Energy Environ.*, **6** (2019) 39.
[43] Yang F. B., Xu L. J. and Huang J. P., *ES Energy Environ.*, **6** (2019) 45.
[44] Xu L. J. and Huang J. P., *Sci. China Phys. Mech. Astron.*, **63** (2020) 228711.
[45] Liu Y. D., Song J. L., Zhao W. X., Ren X. C., Cheng Q., Luo X. B., Fang N. X. L. and Hu R., *Nanophotonics*, **9** (2020) 855.
[46] Song J. L., Huang S. Y., Ma Y. P., Cheng Q., Hu R. and Luo X. B., *Opt. Express*, **28** (2020) 875.